Supplementary Information

Current vortices and magnetic fields driven by moving polar twin boundaries in ferroelastic materials

Guangming Lu[1,2], Suzhi Li[1*], Xiangdong Ding[1*], Jun Sun[1] and Ekhard K. H. Salje[1,2*]

1 *State Key Laboratory for Mechanical Behavior of Materials, Xi'an Jiaotong University, Xi'an 710049, China*

2 *Department of Earth Sciences, University of Cambridge, Cambridge CB2 3EQ, UK*

Corresponding author: lisuzhi@xjtu.edu.cn; dingxd@mail.xjtu.edu.cn; ekhard@esc.cam.ac.uk

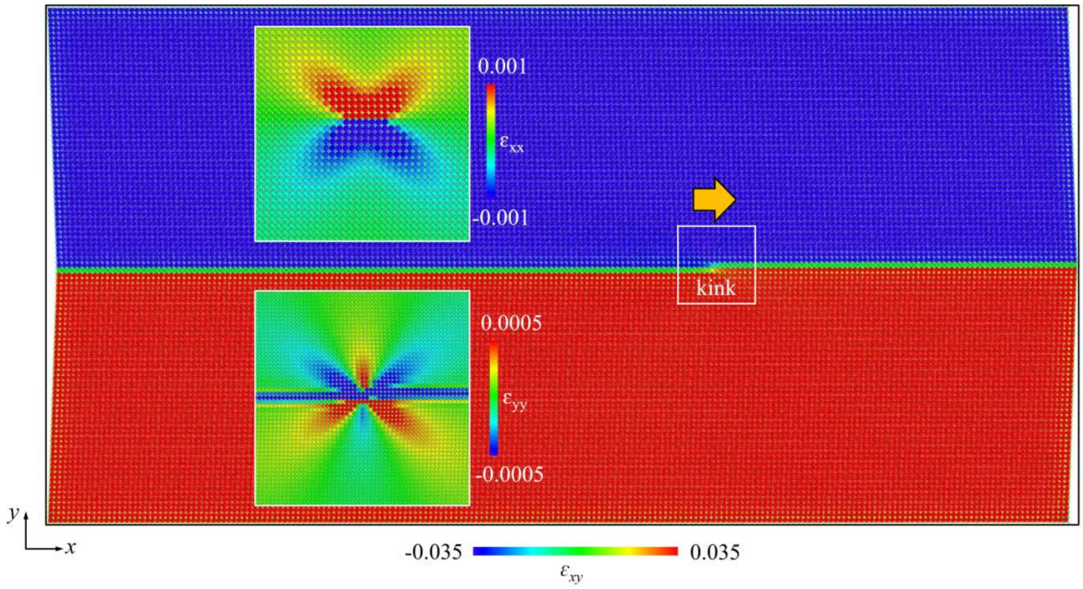

Fig. S1 A moving kink residing inside a horizontal twin wall. The colors are coded according to the atomic-level shear strain. The local strain field of kink shows typical inhomogeneous Eshelby patterns (see the insets).

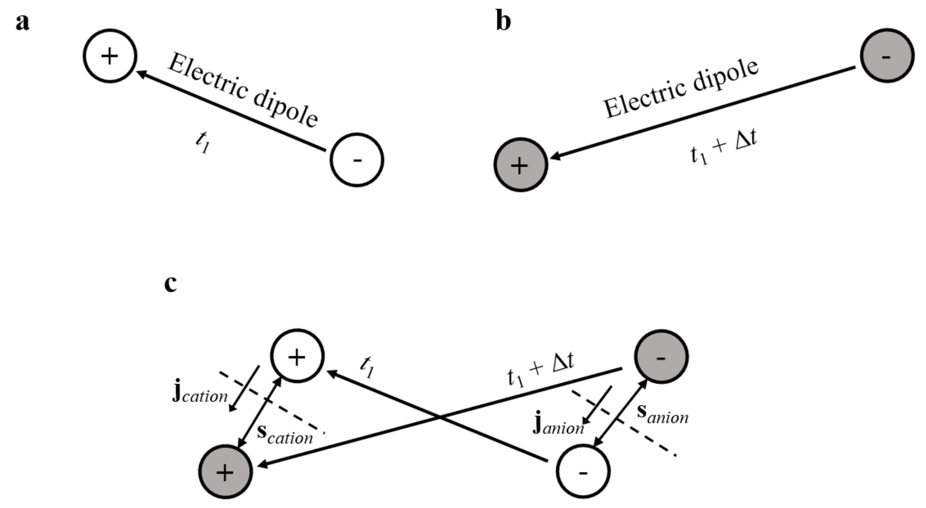

Displacement current density

$$\mathbf{j} = \mathbf{j}_{cation} + \mathbf{j}_{anion} = Q^{+}\mathbf{v}_{cation} + Q^{-}\mathbf{v}_{anion} = Q^{+}\frac{\mathbf{s}_{cation}}{\Delta t} + Q^{-}\frac{\mathbf{s}_{anion}}{\Delta t}$$

Fig. S2 Schematic illustration of calculation of the displacement current density [1, 2, 3]. $\mathbf{j}_{cation}$ and $\mathbf{j}_{anion}$ are the current density contributed by cation and anion. Q^{+} and Q^{-} are the amount of charge carried by cation and anion. $\mathbf{s}_{cation}$ and $\mathbf{s}_{anion}$ are the moving distances of cation and anion during a time interval Δt. $\mathbf{v}_{cation}$ and $\mathbf{v}_{anion}$ are the corresponding velocities.

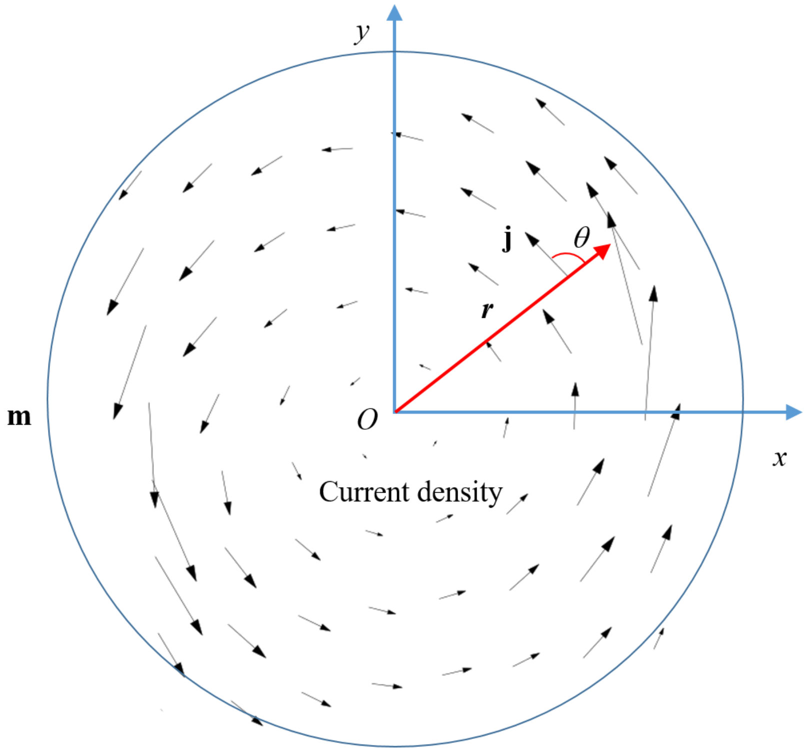

Magnetic moment

$$\mathbf{m} = \frac{1}{2}\sum_i Q_i(\mathbf{r}_i \times \mathbf{v}_i) = \frac{1}{2}\sum_i Q_i|\mathbf{r}_i||\mathbf{v}_i|\sin\theta_i$$

Fig. S3 The calculation of magnetic moment perpendicular to the displacement current [1, 2, 3]. **m** is the magnetic moment perpendicular to the atomic plane contributed by all current density vectors. For the *i*th particle, **r** is the position vector, **v** is the velocity and θ_i is the angel between **r** and **v**.

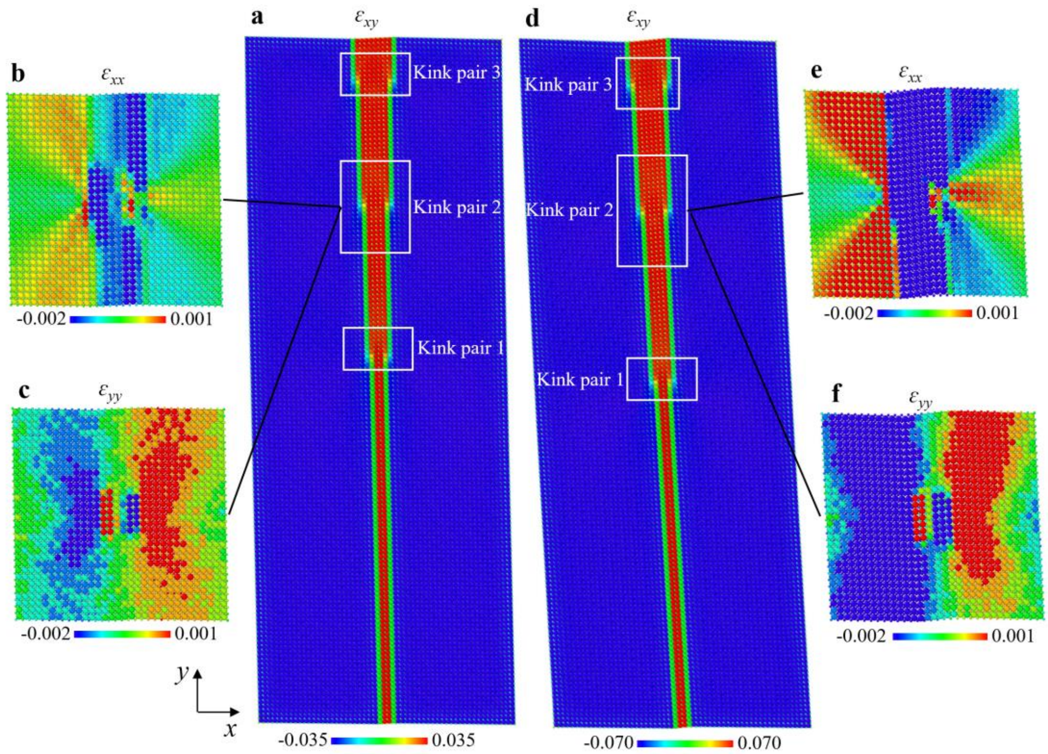

Fig. S4 The atomic configuration of needle domain with three kink pairs at the twin boundaries for the (a)-(c) 2^{o} model and (d)-(f) 4^{o} model. The colors are coded according to the atomic-level shear strain ε_{xy} in (a), (d), normal strain ε_{xx} in (b), (e) and normal strain ε_{yy} in (c), (f). The local strain fields near kink pairs show typical inhomogeneous Eshelby patterns.

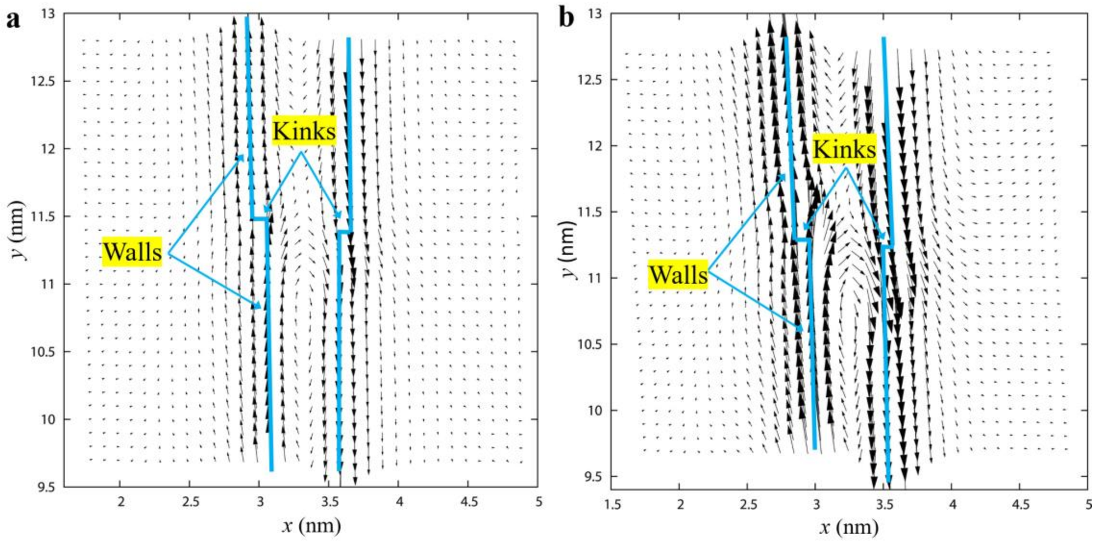

Fig. S5 Comparisons of polar displacements near kink pair for the (a) 2° model and (b) 4° model. The polarization is induced via flexoelectricity. The magnitudes of the polar displacement near the kinks in 4° model is larger than that in 2° model due to the larger inhomogeneous strains. The polar displacements are amplified by a factor of 50 for clarity.

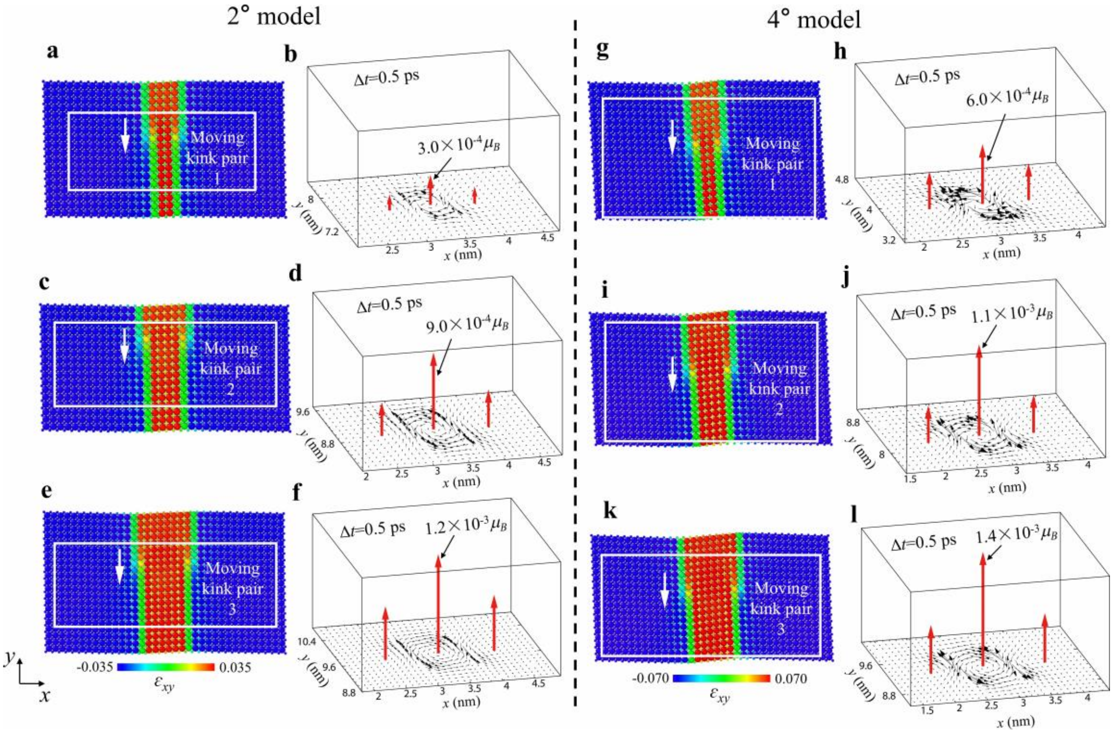

Fig. S6 Displacement currents and the corresponding magnetic fields generated by moving kink pairs for the (a)-(f) 2° model and (g)-(l) 4° model. The colors of the atomic configuration are coded according to the atomic-level shear strain. The current density was calculated using the relative displacements of anions and cations within a time interval of 0.5 ps. The local eddy current was on the order of ~10^{-18}A. The current density in the vector maps are amplified by a factor of 2×10^{17} for clarity.

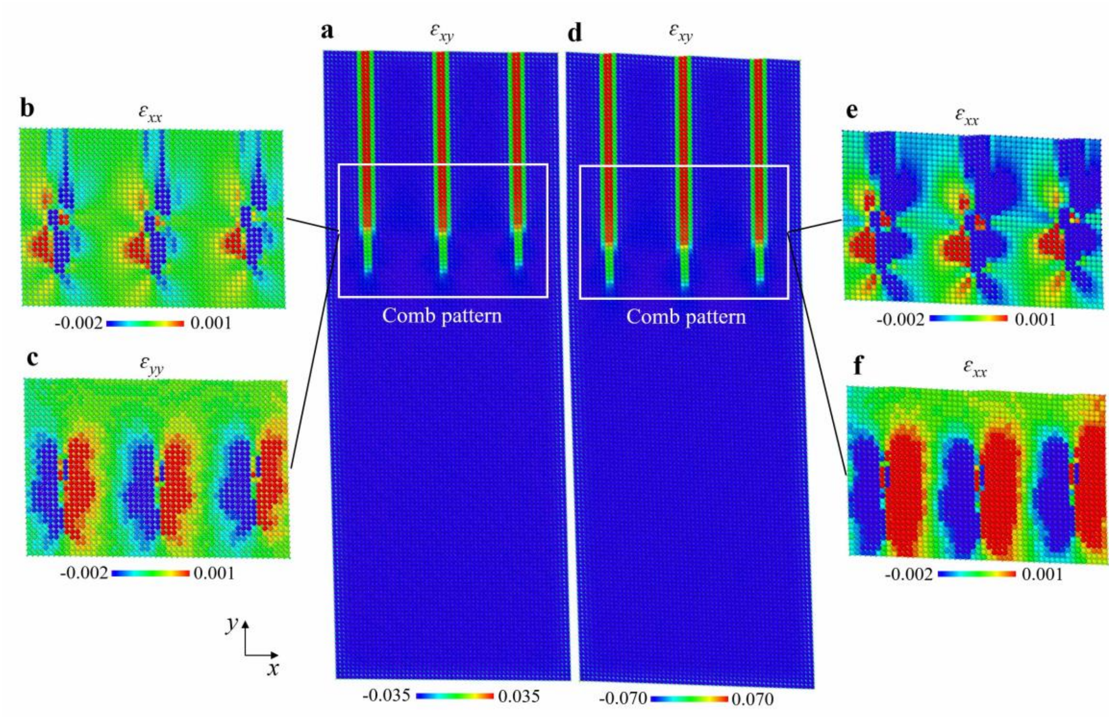

Fig. S7 The atomic configuration of a ferroelastic comb pattern with parallel needle domains for the (a)-(c) 2º model and (d)-(f) 4º model. Every needle has a thickness of 4 atomic layers. The inter-distance between parallel needles is 1.5 nm. The colors are coded according to atomic-level shear strain ε_{xy} in in (a), (d), normal strain ε_{xx} in (b), (e) and normal strain ε_{yy} in (c), (f).

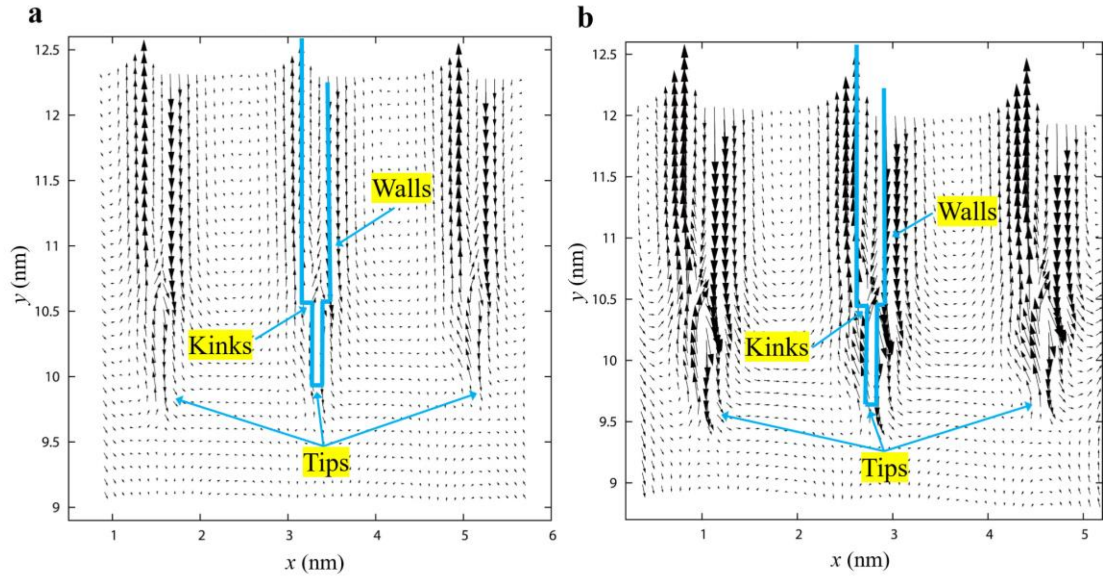

Fig. S8 Comparisons of polar displacements near comb pattern for the (a) 2^o model and (b) 4^o model. The polarization is induced via flexoelectricity. The magnitudes of the polar displacement near the kinks in 4^o model is larger than that in 2^o model due to the larger inhomogeneous strains. The polar displacements are amplified by a factor of 50 for clarity.

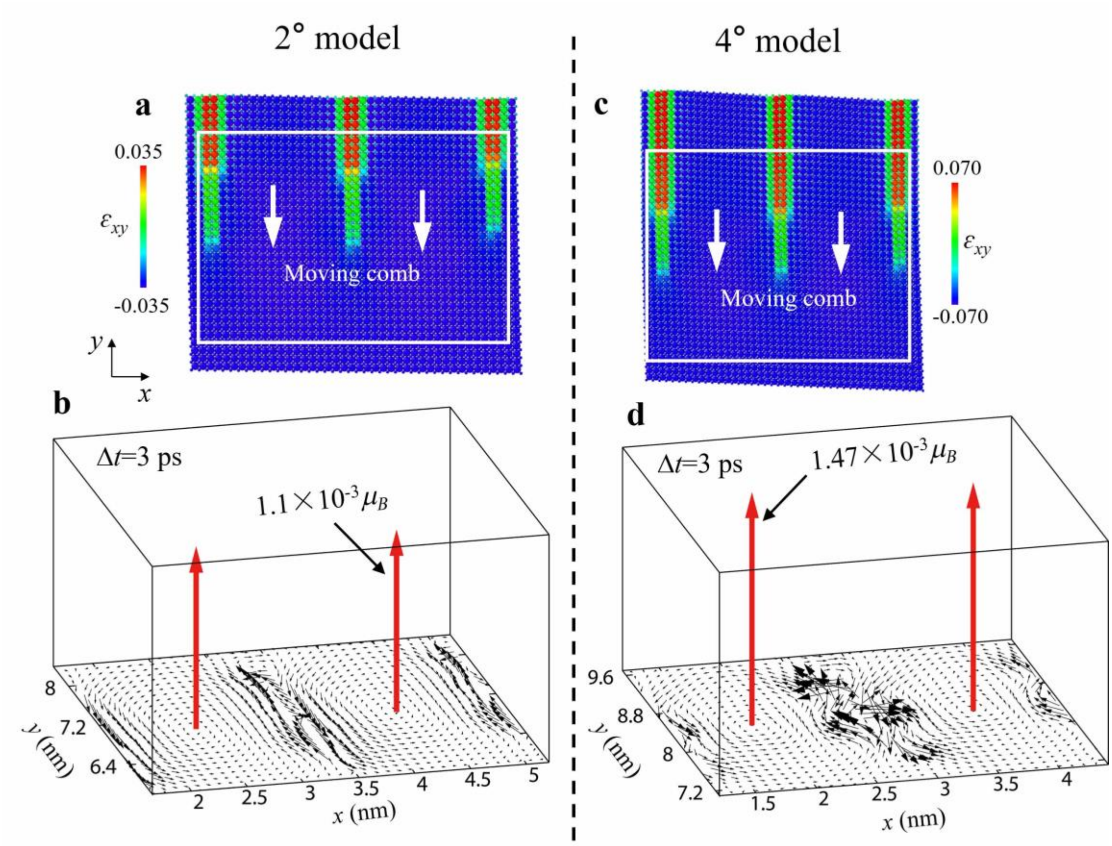

Fig. S9 Displacement currents and the corresponding magnetic fields generated by a moving comb pattern for the (a)-(b) 2º model and (c)-(d) 4º model. The needle is thin with 4 atomic layers for each. The needle distance is 1.5 nm. The colors of the atomic configuration are coded according to the atomic-level shear strain. The current density in the vector maps are amplified by a factor of 1×10^{18} for clarity.

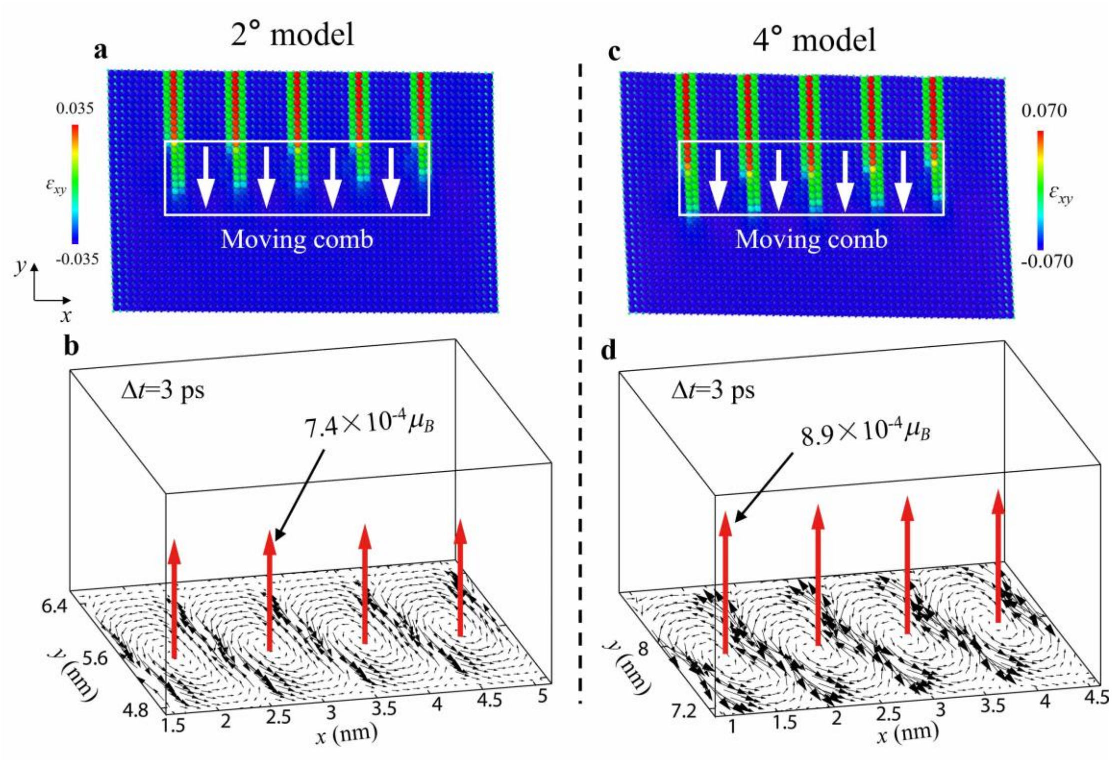

Fig. S10 Displacement currents and the corresponding magnetic fields generated by a moving denser comb pattern for the (a)-(b) 2° model and (c)-(d) 4° model. The needle is thinner with 3 atomic layers for each. The inter-tip distance is shortened to be 0.7 nm. The colors of the atomic configuration are coded according to the atomic-level shear strain. The current density in the vector maps are amplified by a factor of 1×10^{18} for clarity.

Table 1. The parameters of the interatomic potential with shear angle of 2° and 4°

Model	Interactions	Range		Potential form
shear angle of 2°	A-A	Short-range	First NN	$20(r-1)^2$
			Second NN	$-10(r-\sqrt{2})^2+8000(r-\sqrt{2})^4$
			Third NN	$8(r-2)^4$
			Fourth NN	$-10(r-\sqrt{5})^2+5100(r-\sqrt{5})^4$
		Long-range	-	Coulomb interaction, dielectric constant = 100
	B-B	Short-range	First NN	$20(r-1)^2$
			Second NN	$1.5(r-\sqrt{2})^2$
		Long-range	-	Coulomb interaction, dielectric constant = 100
	A-B	Short-range	First NN	$0.5(r-\sqrt{2}/2)^2$
		Long-range	-	Coulomb interaction, dielectric constant = 100
shear angle of 4°	A-A	Short-range	First NN	$20(r-1)^2$
			Second NN	$-10(r-\sqrt{2})^2+2000(r-\sqrt{2})^4$
			Third NN	$8(r-2)^4$
			Fourth NN	$-10(r-\sqrt{5})^2+1300(r-\sqrt{5})^4$
		Long-range	-	Coulomb interaction, dielectric constant = 100
	B-B	Short-range	First NN	$20(r-1)^2$
			Second NN	$1.5(r-\sqrt{2})^2$
		Long-range	-	Coulomb interaction, dielectric constant = 100
	A-B	Short-range	First NN	$0.5(r-\sqrt{2}/2)^2$
		Long-range	-	Coulomb interaction, dielectric constant = 100

References

1. Juraschek, D. M. *et al.* Dynamical Magnetic Field Accompanying the Motion of Ferroelectric Domain Walls. *Phys. Rev. Lett.* **123**, 127601 (2019).

2. Juraschek, D. M., Fechner, M., Balatsky, A. V. & Spaldin, N. A. Dynamical multiferroicity. *Phys. Rev. Mater.* **1**, 014401 (2017).

3. Jackson, J. D. American Association of Physics Teachers (1999).